

# Rare Earth Elements Partition and Recovery During Electrodialytic Treatment of Coal Fly Ash

**Lima, Ana T.; Ottosen, Lisbeth M.**

*Published in:*
Journal of the Electrochemical Society

*Link to article, DOI:*
10.1149/1945-7111/ac56a6

*Publication date:*
2022

*Document Version*
Publisher's PDF, also known as Version of record

Journal of The Electrochemical Society



OPEN ACCESS

# Rare Earth Elements Partition and Recovery During Electrodialytic Treatment of Coal Fly Ash

To cite this article: Ana T. Lima and Lisbeth M. Ottosen 2022 *J. Electrochem. Soc.* **169** 033501



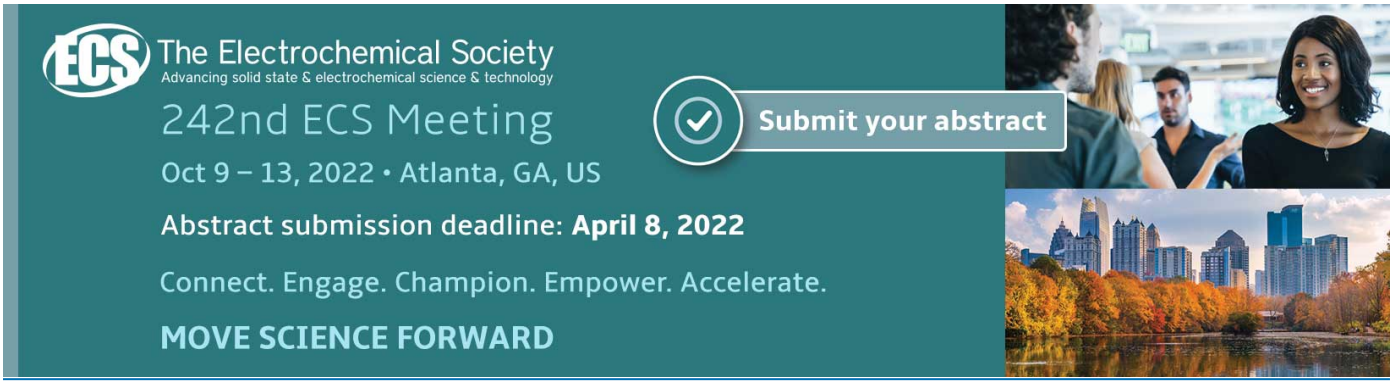

*Journal of The Electrochemical Society*, 2022 **169** 033501

# Rare Earth Elements Partition and Recovery During Electrodialytic Treatment of Coal Fly Ash

**Ana T. Lima**[z] **and Lisbeth M. Ottosen**

*Department of Civil Engineering, Technical University of Denmark, 2800 Lyngby, Denmark*

Rare earth elements (REE) recovery from waste (end-of-line, reusable, recyclable, etc.) should become an essential stream of REE for current demands. Methods to achieve this recovery are then paramount. This study uses the electrodialytic remediation (EDR) as an REE extraction method from coal fly ashes. We used different chemicals to assist REE extraction during EDR: distilled water, 0.01 mol $l^{-1}$ $NaNO_3$, 0.4 mol $l^{-1}$ Sodium acetate in 1.0 mol $l^{-1}$ Acetic acid, and 0.5 mol $l^{-1}$ Citric acid. Citric acid achieved the highest REE extraction/recovery from the four studied solutions: up to 40%. This represents a total recovery of 148 g REE from 1 ton of coal ashes. The citric acid experiment also proved to be energy efficient, using 70 Wh per 100 g of treated coal ash. The acidic environment provided by the citric acid supplies higher REE migration rates towards the cathode. Once at the cathode compartment, REEs then precipitate at the cathode complexed as Ca- and P-bearing minerals.
 [DOI: 10.1149/1945-7111/ac56a6]

Manuscript submitted December 8, 2021; revised manuscript received January 31, 2022. Published March 3, 2022. *This paper is part of the JES Focus Issue on Women in Electrochemistry.*

Supplementary material for this article is available online

REE are highly valuable resources used in various low-carbon energy production intrinsic components, such as batteries, light-emitting diodes, and glass.[1–3] But because REEs have been extensively mined in recent years and demand continues to rise, they are becoming scarce due to conventional ore exhaustion.[4] Despite current REE recycling (from end-of-life wastes, urban mining) only accounting for 1% of used REEs,[5] the latest estimates claim REE quantities contained in secondary sources could meet current global demand even at low extraction yield rates.[6] High technological products are reaching the same constitution as most environmental and waste components: extreme dilution. With extreme dilution, some fundamental limitations are reached for metal recovery.[7] This adds to our already limited capacity to recycle metal from end-of-life products, usually below 10%–20%.[8,9] In the case of extreme dilution, traditional extraction techniques such as pyrometallurgy, precipitation, and solvent extraction become less practical.[7] Because of ore over mining and its nefarious consequences on human and environmental well-being,[10] secondary resources have been indicated as sustainable REE sources,[9,11] such as coal fly ashes.

Technologies for metal recovery from dilute feedstocks are sorely needed.[12] Recycling current technological devices, urban mining, and other circular economy approaches depend on such extraction technologies. Successful separation technologies will be those that can recover metals with high energy efficiency[13] with good yield and purity, adding additional value by simultaneously recovering multiple metal values from the same stream.[7] One of these technologies may be electrodialytic remediation, which has been investigated previously to recover REE.[14,15] EDR was initially a remediation technology, but recent research has focused on using the tool for resource recovery. It uses an applied electrical field, combined with ion-exchange membranes, to a suspension slurry (usually with ashes, contaminated soil, or other hazardous waste), with the purpose of solubilizing and mobilizing ions. These ions are then transported to the cathode (or anode) compartment, where they are deemed extracted (and recovered) from the waste material they were initially bound to. Such ions can be heavy metals,[16] REE,[15] nutrients as phosphorous,[17] among others.

Coal fly ashes are a good source of critical elements such as Ge, U,[4,18] including REE.[2,19,20] Coal ashes have been widely investigated and utilized, especially as cement replacement in concrete,[21,22] but have been recently pointed out as a waste resource-rich in REE.[23] These ashes have been investigated for REE recovery by $H_2SO_4$ leaching,[24] $HNO_3$ leaching,[25] multistage resin-in-leach,[26] and electrodialytic (EDR),[14] with recovery rates as high as 70% REE in EDR.[14] The species or form of REE after extraction is key for REE downstream reuse. Figure 1 depicts the different processes ore undergoes to achieve an acid dissolved form of REE. The steps to achieve REE dissolution are similar in ore and end-of-life products.[27–29] Based on De Michelis,[30] REE should be dissolved in HCl or oxalic acid before being removed from the acidic solution using a ligand in a multi-stage solvent (ethanol) extraction process.[28] Then, REEs are calcined (at 700 °C for 4 h) to obtain REE in the form of oxides.[30] At the acid dissolved stage (Fig. 1), we expect REE to be when undergoing EDR extraction (and recovery). Figure 4 When it comes to resource recovery or elemental recovery, terms are used fluidly,[31] where recovery simply means a separation of metals or nutrients from the waste material. In EDR studies, we usually consider a (elemental) resource recovered once removed and isolated from the waste undergoing treatment. This normally indicates that the (elemental) resource has transposed one of the ion-exchange membranes and can then be found at one of the electrode compartments—being it the anode or cathode compartments. Examples of this are.[14,32–34] The term "Metal extraction" has been used previously in EDR,[35] and it may be a better indication of the process occurring during EDR. To better understand REE extraction during EDR and evaluate its potential for recovery, we used coal fly ash and carried out several EDR experiments with previously tested chemical solutions.[14,36] Specifically, we look at REE partition in the EDR cell at the end of experiments to evaluate REE recovery potential.

## Materials and Methods

***Characterization techniques.—*** *Solutions and electrolytes.*—The pH and electrical conductivity (EC) were determined using distilled water in a liquid-to-solid ratio of 2.5 with Radiometer analytical electrodes. REE quantified in aqueous samples—Y, La, Ce, Pr, Nd, Sm, Eu, Gd, Tb, Dy, Ho, Er, Tm, Yb, and Lu –, were measured on a Perkin Elmer NexION 350D Inductive Coupled Plasma-Mass Spectrometer (ICP-MS).

*Coal fly ashes.*—One sample (approximately 4 kg) of coal fly ash was retrieved from the Amager Power Station, Copenhagen, Denmark. Amager power station is a retired 333 MW coal-fired power station, burning biomass as of 2020. The combustion plant

[z]E-mail: atmli@byg.dtu.dk; lima.at@gmail.com

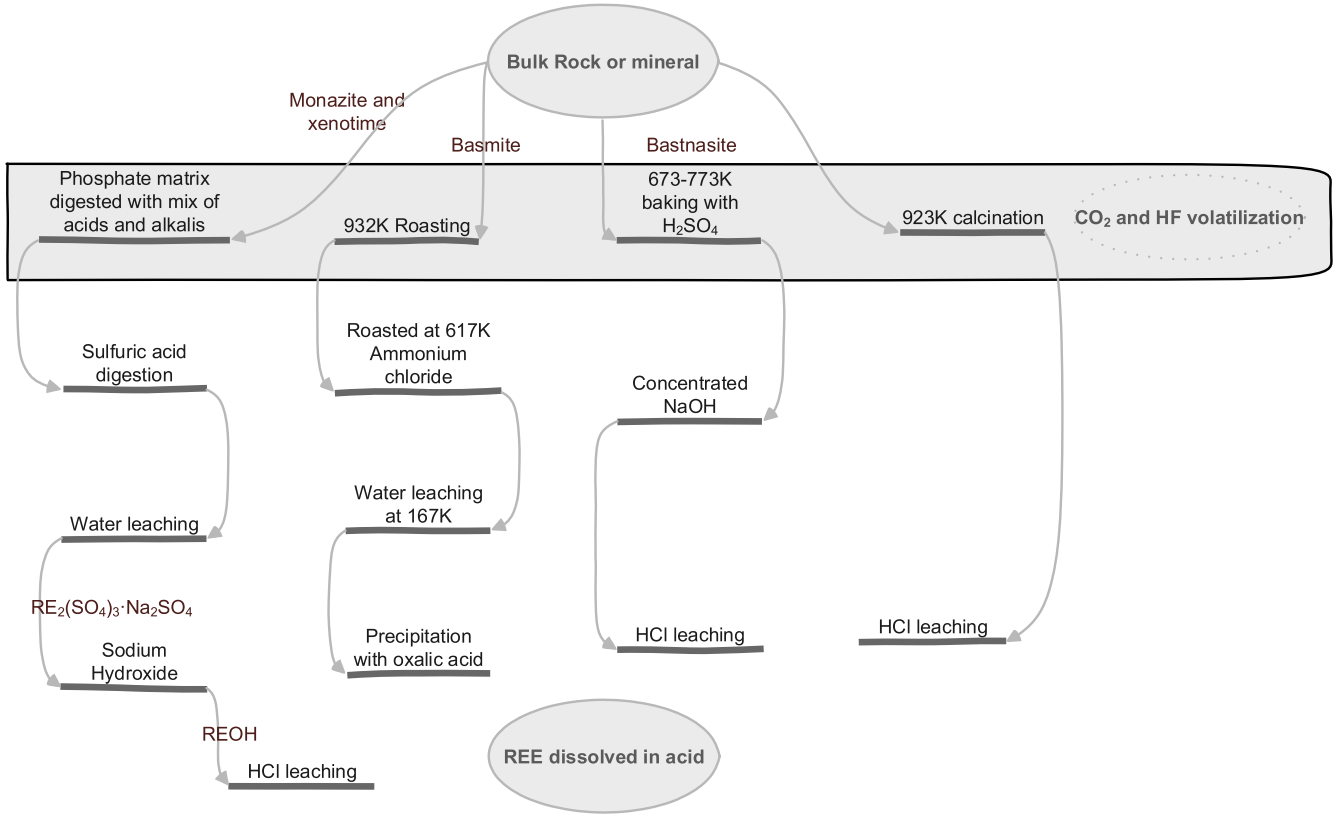


**Figure 1.** REE extraction diagram after ore mining consisting of different extraction combinations to achieve the final REE in acid form.[30]

burns coal at a temperature of 440 °C. We collected coal fly ashes in March 2020. Organic matter (OM) was calculated based on the mass loss at 550 °C using a muffle furnace for 1h. The total carbonate content was also calculated based on loss on ignition (LOI) at 950 °C for 1h. The mass loss relative to OM content (loss at 550 °C) was duly subtracted. Coal fly ashes water content was also deducted (weight loss at 105 °C). All analyses were done in triplicate.

To measure the total concentrations in the various wastes, 0.25 g of coal fly ashes were digested in an Anton-Paar Multivave 3000 microwave using USEPA 3052 method with 6 ml $HNO_3$ 65%, 2 ml HCl 30%, and 2 ml HF 40% all of the supra-pure grade. Certified reference materials stream sediment and lake deposit GBW 07318 were used. All samples were filtered with a 0.45 $\mu$m filter before analysis. Al, As, Ba, Cd, Cr, Cu, Fe, K, Mg, Mn, Na, Ni, P, Pb, S, and Zn concentrations in the wastes and sediments were measured in an Agilent ICP-OES Varian 720ES. REE Sc, Y, La, Ce, Pr, Nd, Sm, Eu, Gd, Tb, Dy, Ho, Er, Tm, Yb, and Lu, were measured on a Perkin Elmer NexION 350D Inductive Coupled Plasma-Mass Spectrometer (ICP-MS). Promethium (Pm) can only be artificially synthesized and does not occur in nature,[37] so we excluded it from this study. Data were processed in the Syngistix™ software (v. 2.1).

$NO_3^-$, $Cl^-$, and $SO_4^{2-}$ anions were all analyzed by a Dionex-120 Ion Chromatograph after having the wastes/sediments suspended in distilled water in a liquid-to-solid ratio of 2.5 for 12 h. The same solution was used to determine REE water solubility. In addition, coal fly ashes where brought together with 0.01 mol $l^{-1}$ $Na_2SO_4$ in a liquid-to-solid ratio of 2.5 for 12 h to determine REE solubility in $Na_2SO_4$. These solutions were taken for analysis in the ICP-MS described above.

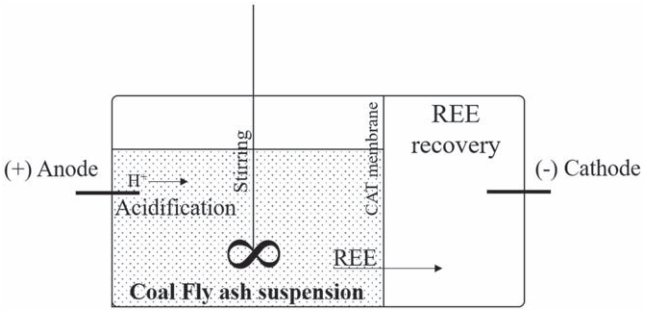


**Figure 2.** Schematic representation of EDR treatment for REE recovery from coal fly ashes.

***EDR experiments.***—Coal fly ash treated by in EDR were pre-treated with 0.01 mol $l^{-1}$ $NaNO_3$, pH2: 2 kg of coal ash were put in contact with 2 l 0.01 mol $l^{-1}$ $NaNO_3$, pH2, in a ratio of 1:1, for 24 h.

Two-compartment EDR cells were used in this study, as described in. Ref. 38. The anode is in direct contact with the coal fly ash suspension while the cathode is placed in the adjacent (cathode) compartment (Fig. 2). The setup uses the $H^+$ production at the anode to acidify the coal fly ash and mobilize strongly bound elements towards the cathode (if positively charged, such as the case of REE). The Plexiglas cell has a 10 cm long anode compartment and 5 cm long cathode compartment, with an internal diameter of 8 cm. An IKA RW11 Basis Lab Egg motor (app. 1500 rpm) kept the suspension bystirring a glass rod stirrer with a flexible plastic flap attached, and a Pan World Magnet pump was used to circulate the catholyte. 3 mm diameter Permascand platinum-coated titanium electrodes were fed by a Hewlett Packard E3612 A power supply, maintaining a constant electric DC current of 60 mA. An Ionics CR67 HUY N12116B cation exchange membrane separated the two compartments. The same electrodes described in 2.2.1 were used to monitor pH and EC in the suspension and electrolytes. The experimental design is described in Table I. Room temperature is constant throughout the year, around 21 °C.

Coal ashes previously in suspension during the experiments were filtered through a 45 $\mu$m filter and air-dried for 48 h after EDR

**Table I. Experimental design of the electrodialytic experiments. The chemical solutions used in Coal#3 and Coal#4 were adopted from Refs. 36. and, 15 respectively.**

| Experiment | Solution added to ash | Catholyte | Experimental duration (days) |
|---|---|---|---|
| Coal#1 | Distilled water | 0.01 mol $l^{-1}$ $Na_2SO_4$, pH2 | 7 |
| Coal#2 | 0.01 mol $l^{-1}$ $NaNO_3$, pH2 | 0.01 mol $l^{-1}$ $Na_2SO_4$, pH2 | 7 |
| Coal#3 | 0.4 mol $l^{-1}$ Sodium acetate in 1.0 mol $l^{-1}$ Acetic acid | 0.01 mol $l^{-1}$ $Na_2SO_4$, pH2 | 9 |
| Coal#4 | 0.5 mol $l^{-1}$ Citric acid | 0.01 mol $l^{-1}$ $Na_2SO_4$, pH2 | 9 |

experiments. The remaining liquid—Ash M—was then analyzed for REE contents. Coal ashes were then submitted to the tests described in 2.2.2 for further analysis. The membranes and stirrer were placed in 1 mol $l^{-1}$ $HNO_3$ and the electrodes in 5 mol $l^{-1}$ $HNO_3$, respectively. A piece of the membrane was cut at the end of the experiment and digested. All liquid samples, including suspension liquid and catholyte, were analyzed for REE contents.

***Electrode.—***After the EDR experiments, electrodes (as illustrated in Fig. 3) were air-dried for 48 h. Once dried, the electrode coating was powdered and analyzed by a PANalytical X'Pert Pro X-ray powder diffraction (XRD) to identify major crystalline phases. The instrument operated at 45 mA and 40 kV applying Cu Kα radiation with a 2Θ X'Celerator detector. The samples were scanned in the range of 4–100 2 Θ 4 within 2.5 h. The diffractograms were interpreted using the ICDD PDF-4 database for minerals, and the main peaks were identified.

Coal#4 was replicated to study the electrode in detail. We preserved the electrode with vacuum-impregnated low-viscosity epoxy resin, polished with diamond discs of 220–1 $\mu$m at 150 rpm using ethanol as a lubricant, as described in Ref. 39. Electrode layers and elemental mapping were done by a Zeiss Ultra Plus field emission scanning electron microscope (ESEM) instrument (Oberkochen, Germany) at a 20 kV accelerator voltage and a working distance of 8–10 mm, coupled to an Oxford EDX detector (Oxford Instrument, Oxfordshire, the UK). The cross-section of the electrode was coated with a layer of 80 nm carbon.

***Data treatment.—***REE concentrations developing with time were collected experimentally, and then analysed with the remaining Al, As, Ba, Cd, Cr, Cu, Fe, K, Mg, Mn, Na, Ni, P, Pb, S, and Zn time-series. A Principal Component Analysis (PCA) was adjusted using SIMCA 16 (Sartorius Stedium Biotech). PCA reduces datasets with many interrelated variables while retaining the variation presented in the original data as much as possible. This reduction is achieved by transforming the actual variables into a new set of variables, the principal components, which are uncorrelated linear combinations of the variables, and that can be visualized. Generally, the distance between a point and the origin (of x and y axes), corresponding to a vector, is proportional to the relative importance of the variable in the PCA model. Points that are close together in a plot and that their vectors form acute-angled are significantly correlated. This means that the closer the points are together, the higher the correlation. If vectors form 90° angles, then variables are not correlated, while variables that include 180° angles are considered negatively correlated—more details in Ref. 40.

***Energy consumptium.—***The energy consumption can be calculated as described in Ref. 41.

$$E = \int_{t_0}^{t_f} V(t)I(t)dt \qquad [1]$$

where $E$ is the energy consumption (Wh), $V$ is the voltage variation between electrodes (V), $I$ is the current (A), and $t$ is the duration (h). DC current is constant, as described in Section 2.2, and voltage was obtained by averaging the daily obeservations.

## Results and Discussion

***Characteristics of investigated coal fly ash.—***The main characteristics of the investigated coal fly ash are presented in Table II. The main characteristics of coal ash are in line with previous studies,[42,43] including REE contents. Here, the coal ashes are equivalent to what is specified in the literature as brown[42] and/or anthracite.[14] Mineral identified in the coal fly ashes were mullite ($3Al_2O_3{\cdot}2SiO_2$), quartz ($SiO_2$), calcite ($CaCO_3$), and hematite ($Fe_2O_3$) (Fig. S1 (available online at stacks.iop.org/JES/169/

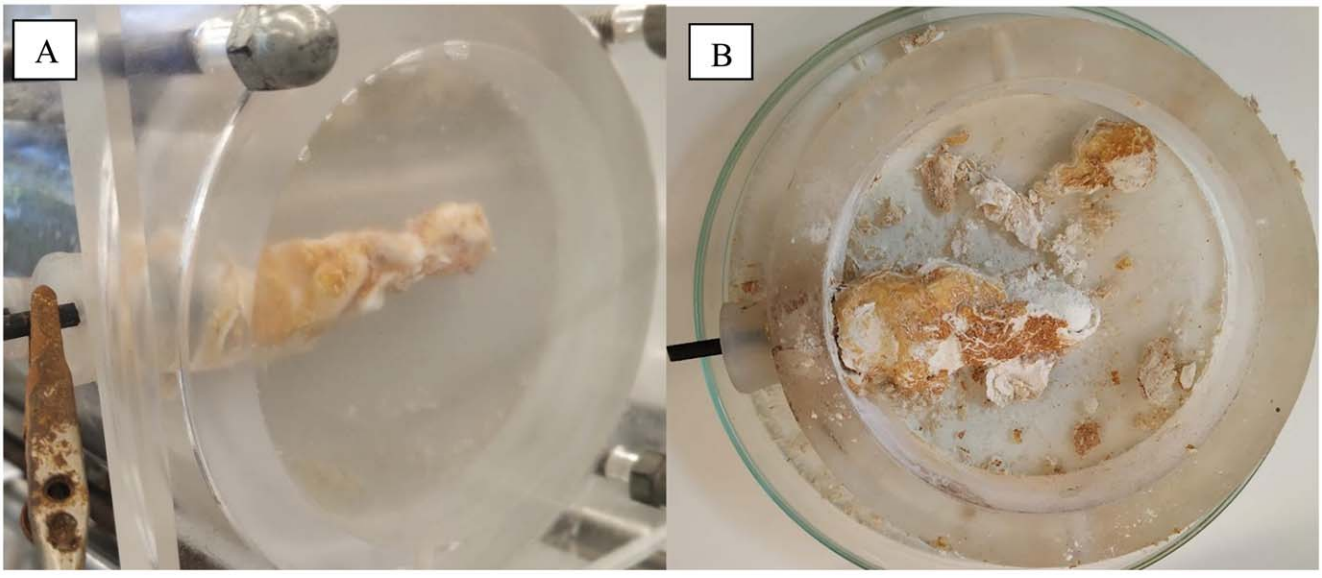


**Figure 3.** Electrode illustration during Coal#4 (A) and after drying for 48 h (B).

**Table II. Summary of coal fly ashes characteristics. Bold REE highlight critical REEs, as defined in Ref. 18.**

| Various characteristics | Coal fly ash | REE total concentration | Coal fly ash |
|---|---|---|---|
| Al (g $kg^{-1}$) | 7.20 ± 0.17 | Y (mg $kg^{-1}$) | 43.5 ± 2.61 |
| Ca (g $kg^{-1}$) | 16.24 ± 0.18 | Nd (mg $kg^{-1}$) | 52.7 ± 2.1 |
| Fe (g $kg^{-1}$) | 14.81 ± 0.47 | Eu (mg $kg^{-1}$) | 2.25 ± 0.10 |
| K (g $kg^{-1}$) | 0.50 ± 0.02 | Tb (mg $kg^{-1}$) | 1.45 ± 0.08 |
| Mg (g $kg^{-1}$) | 4.02 ± 0.03 | Dy (mg $kg^{-1}$) | 8.59 ± 0.50 |
| Mn (g $kg^{-1}$) | 0.18 ± 0.00 | Er (mg $kg^{-1}$) | 4.88 ± 0.31 |
| Na (g $kg^{-1}$) | 0.38 ± 0.01 | Ce (mg $kg^{-1}$) | 125.0 ± 5.3 |
| P (g $kg^{-1}$) | 1.96 ± 0.03 | Gd (mg $kg^{-1}$) | 9.93 ± 0.56 |
| Organic content (%) | 2.05 ± 0.14 | La (mg $kg^{-1}$) | 64.6 ± 2.9 |
| Carbonates (%) | 0.57 ± 0.14 | Pr (mg $kg^{-1}$) | 15.1 ± 0.60 |
| Cl (mg $kg^{-1}$) | 0.02 ± 0.00 | Sm (mg $kg^{-1}$) | 10.9 ± 0.49 |
| $NO_3$ (mg $kg^{-1}$) | 4.86 ± 0.40 | Ho(mg $kg^{-1}$) | 1.69 ± 0.11 |
| $SO_4$ (mg $kg^{-1}$) | 4.27 ± 0.08 | Lu (mg $kg^{-1}$) | 0.67 ± 0.04 |
| pH | 11.45 ± 0.02 | Sc (mg $kg^{-1}$) | 22.1 ± 1.22 |
| Conductivity (mS $cm^{-1}$) | 3.04 ± 0.04 | Tm (mg $kg^{-1}$) | 0.70 ± 0.05 |
| | | Yb (mg $kg^{-1}$) | 4.56 ± 0.34 |

033501/mmedia)). This is per what was found in other studies using the same ashes,[43] and comparable to other coal fly ashes.[44,45] The coal ashes were pre-treated before EDR: they were prewashed with 0.1 mol $l^{-1}$ $Na_2SO_4$, pH 2. As observed in Fig. S1, coal fly ash minerals remained the same and were not altered by this procedure.

***EDR of REE.—***The pre-treated fly ashes were submitted to four EDR experiments as described in Table I. REE distribution in the EDR cell at the end of experiments is depicted in Fig. 4. REEs found at the cathode compartment are considered extracted or recovered (see Fig. 2). Here, REEs are mainly found precipitated at the cathode. Coal#4 was the most successful experiment in recovering REEs, followed by Coal#1. Coal#4 uses 0.5 mol $l^{-1}$ Citric acid as the chemical solution to help desorb REEs from coal ash because it forms stable complexes with trivalent REEs, as previously used in.[15] With citric acid, REE recovery can amount to 40% in the case of Gd and Tb—Tb being considered a critical REE.[18] However, it is noted that EDR where the coal ash was suspended in distilled water (Coal#1), gave relatively good results, with up to 20% recovery (Fig. 4). Even though we used higher current intensities, these recovery estimates are much lower than described in Ref. 14. Perhaps comparison is unsubstantiated as different pre-treatments were used in the two studies. Coal#3, using 0.4 mol $l^{-1}$ sodium acetate in 1.0 mol $l^{-1}$ acetic acid as desorbing agent, showed poor REE recovery (Fig. 4), contrary to previous experiments.[36] Citrates possess the highest stability among organic acids (e.g. log $\beta = 7.7$ for Nd citrate).[46] Nd acetate has a lower stability constant (log $\beta = 6.7$),[47] explaining why Coal#4 was more successful.

In this study, REE was found strongly bound to the coal fly ashes at the end of experiments, independent of experimental conditions (Fig. 4). "Ash M" is the abbreviation for the liquid part of the stirred suspension in the anode compartment (see Fig. 2). We can observe that REE found in "Ash M" at the end of the experiments are 100 to 1000 fold higher than concentrations found in distilled water and

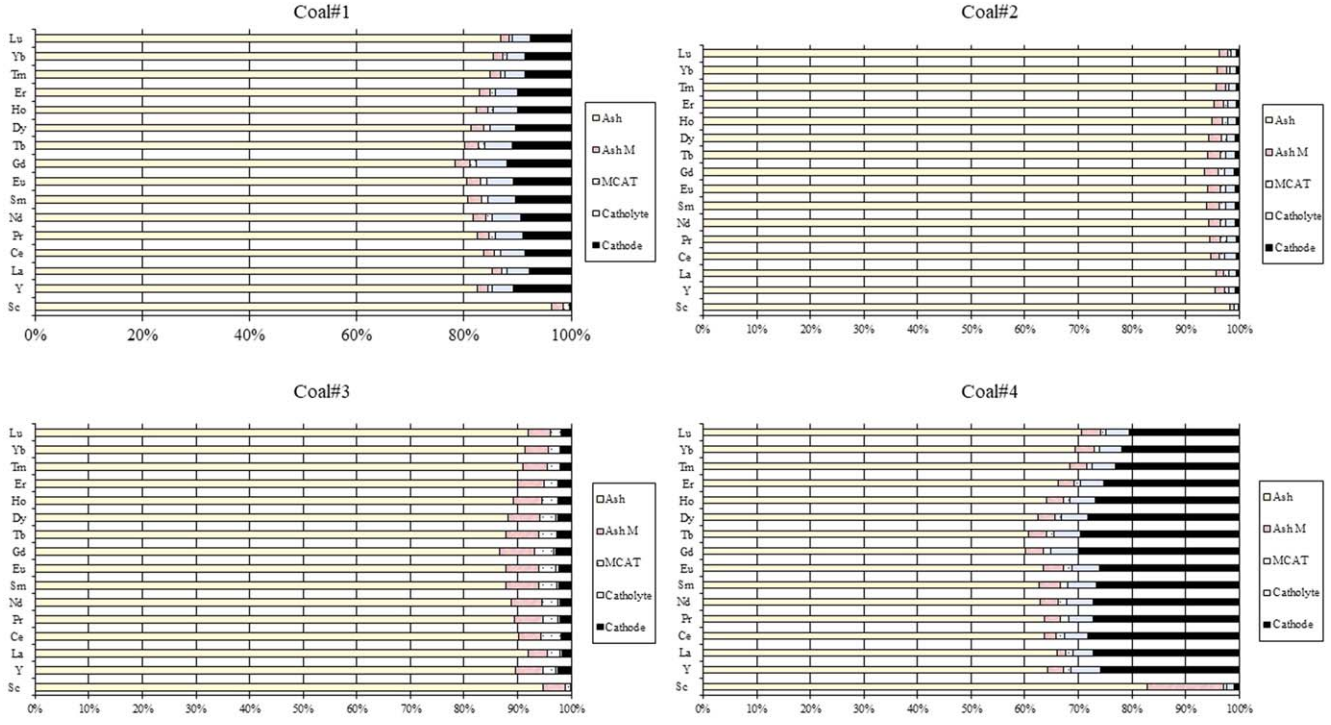


**Figure 4.** Depiction of REE partition in the EDR cell at the end of the four experiments. Legend: MCAT- Cation-exchange membrane.

0.01 mol $l^{-1}$ $Na_2SO_4$ (Table III)—depending on the REE in question. REE dissolution from coal ashes is then enhanced by the constant supply of $H^+$ at the anode,[48,49] an experimental setup already proposed previously by Pedersen et al.[50] Once extracted, we find REE deposited at the electrode (Fig. 4) although previous studies have claimed REE to be extracted in dissolved form in the catholyte solution.[14] The following sections explore REE form and speciation in each medium: catholyte and electrode deposit.

***Electrolytes and dissolved REE migration during EDR.—*** Experiments Coal#1 to Coal#3 showed REE in the catholyte after one day of EDR experiment (Figs. 5a–5c), independent of the solution used to aid the desorption of REE (solutions described in Table I). Coal#4, which used 0.5 mol $l^{-1}$ Citric acid as desorbing solution during EDR, only showed breakthrough after 2.5 d of the experiment (Fig. 5d). But from the performed experiments, only Coal#4 showed a regular breakthrough pattern, i.e. a rise in concentration after a few days of experiment with a noticeable decline after peak concentration (Fig. 5). All other experiments (Coal#1 to Coal#3) showed several REE release peaks, indicating that REE desorption from minerals occurs at different stages in these experiments. pH in Ash M is comparable in all experiments (reaching pH 2 roughly after 3 d of experiment). Interestingly, catholyte pH reached 3 after 6 d of experiment in Coal#1, 3 d in Coal#4, and never reached acidic conditions in Coal#2 or Coal#3 (pH data not shown).

***Legend.—***To understand which minerals may be responsible for REE dissolution, we performed a PCA with the time-series of REE, as well as Al, As, Ba, Cd, Cr, Cu, Fe, K, Mg, Mn, Na, Ni, P, Pb, S, and Zn, to understand which elements were showing up at the cathode simultaneously—or at least statistically significantly (Fig. 6). Besides the high correlation between REEs, we can observe two groups sitting closer to the REE group: Mn and Cu, and Al and Cr. REE in soils can be mainly bound to organic matter and Fe, Al, and Mn oxides.[51] But coal fly ashes are a very different material than soil, with no active organic matter but high contents of all Fe, Al, and Mn elements (Table II). Nevertheless, Fe does not seem to significantly desorb at the same as the REE during EDR (Fig. 6). The most crystalline Al-mineral in the studied coal fly ashes was the aluminosilicate mullite ($3Al_2O_3{\cdot}2SiO_2$) (Fig. S1), suggesting that this mineral can be scavenging most REEs. This agrees with Pan et al.,[19] who estimated a 98% correlation between Al and REE in coal ashes. In this study, we see that Al and Cr correlate significantly, suggesting that Cr desorbs from an aluminosilicate mineral during EDR. Since Cr displays an excellent correlation with Al, particularly $Al_2O_3$,[52] this is likely. But overall, REEs present in coal fly ashes remain in residual minerals such as silicates or oxide form.[53] In this study, we observe Mn (and Cu) highly correlating with REE, suggesting that EDR can extract REEs that are scavenged in Mn oxide minerals (Fig. 6).

Studies have suggested that REEs can be extracted in their ionic form[36] because they are easily hydrolyzed.[54] Indeed, Coal#1 uses deionized water and presents high mobility of REE through experimental time—to the same extent as concentrations experienced during Coal#4 (the experiment with 0.5 mol $l^{-1}$ Citric acid as desorbing solution). To understand better REE ions migration during EDR, we calculated the migration flow vector of the species ($J_i^m$) (mol $cm^{-2}$ $s^{-1}$), which is given by

$$J_i^m = -u_i^* \times C_i \times \nabla(E) \quad [2]$$

where $u_i^*$ corresponds to the effective ionic mobility ($cm^2$ $V^{-1}$ $s^{-1}$), $C_i$ is the concentration of electroactive species in Ash_M (mol $l^{-1}$), and $\nabla(E)$ is the gradient vector of the electric potential (V $cm^{-1}$).[55] The effective ionic mobility is given by

$$u_i^* = \frac{D_i^* z_i F}{RT} \quad [3]$$

$D_i^*$ refers to the diffusion coefficient of species $i$ ($cm^2$ $s^{-1}$), $z_i$ is the ion valence, $F$ is the Faraday constant, $R$ is the universal gas constant, and $T$ is the temperature of the reaction medium.[55] All equation parameters are listed in Table IV and can be derived from Tables III and IV. Table V summarizes the highest and lowest $J_i^m$, as well as the corresponding REE. REE diffusion coefficients in aqueous solutions were retrieved from Liyanandirah et al.,[56] but Y and Lu are not available. We decided to explore REE individually and show how dependent of REE concentration (solubility) $J_i^m$ is, spanning across 3 orders of magnitude while $u_i^*$ remains within one order of magnitude. The electric field strength $\nabla(E)$ is also key to achieve higher $J_i^m$, but since our experimental setup was designed to study the influence of solution, the electric field was maintained (more or less) constant. In fact, we applied constant current while the electric field was monitored (data not shown but summarized in Table V).

Comparing REE ionic mobility $u_i^*$ with classical physical chemistry literature ($3{\cdot}10^{-9}$ to $1{\cdot}10^{-8}$ $m^2$ $s^{-1}$ $V^{-1}$ in Ref. 57), we conclude that REE displays low ionic mobility ($6–7{\cdot}10^{-11}$ $m^2$ $s^{-1}$ $V^{-1}$ in Table IV). In this study, we consider aqueous REE diffusion coefficients,[56] with lower diffusion capacity than major elements (such as Ca or Na) typically used in soil studies Ref. 57. But comparing to studies looking at REE mobility, $J_i^m$ is on the higher side ($3.5{\cdot}10^{-11}$ compared to $1.8{\cdot}10^{-10}$ mol $cm^{-2}$ $s^{-1}$ in Ref. 36). This is remarkable if we consider that the diffusion coefficient adopted by Pires et al.[36] for Y was referring to Sc, one order of magnitude higher than the ones used in this study (Table IV), and the electric field was identical (4 to 11 V in Ref. 36.). It is worth noticing that the EDR cell offers (nearly) perfect mixing and favors ion desorption of the solid phase, as observed by Lima et al.,[58] where issues of tortuosity and coupled flow are minimized and ion mobility approaches that of ideal solutions. In suspended EDR, the ionic mobility of $H^+$ ions could be approximately estimated as its value in aqueous solution, which is $3625{\cdot}10^{-6}$ $cm^2$ $V^{-1}$ $s^{-1}$.[49] Overall, Sc, Ce and Nd present the highest migration $J_i^m$ (Tables V, IV), particularly when assisted by citric acid in experiment Coal#4. The use of citric acid as assisting solution provides REE high solubility. Trivalent REE form the strongest complexes with O-donor groups such as carboxylate, and citric acid is composed of three carboxylate groups (CH3COO-).[59] As seen in Fig. 1, acidic (HCl or oxalic acid) extractions are a mandatory step in ore processing to achieve REE in a dissolved form. Placing the anode in the ash compartment is a strategy used previously by Kirkelund et al.[38] to acidify alkaline ashes and obtain high metal desorption from them. Indeed, Coal#1 used this strategy and achieved relatively high $J_i^m$ (Tables V, IV). Nevertheless, the citric acid enhanced environment provided Coal#4 a higher REE $J_i^m$ migration rate and a higher REE recovery at the end of the experiment (Fig. 4).

***Electrode deposition.—***Coal#4 shows the highest REE content deposited at the electrode (Fig. 4). To understand how REE are found in the electrode precipitate, we performed XRD analysis (Fig. 7) and ESEM visualization (Fig. 8). Coal#1 electrode showed the most diverse minerals: Iron Sulfate hydroxide ($FeHO_5S$), Calcium hydroxide $Ca(OH)_2$, carbonate Green rust ($[Fe^{2+}{}_4Fe^{3+}{}_2(HO^-)_{12}]^{2+}$ $[CO^{2-}{}_3{\cdot}2H_2O]^{2-}$), Calcite ($CaCO_3$), and Brushite ($CaHPO_4{\cdot}2H_2O$). All Coal#2, Coal#3 and Coal#4 did not show this high mineral variability, where only Iron Sulfate hydroxide ($FeHO_5S$), Calcium hydroxide ($Ca(OH)_2$), and Calcite ($CaCO_3$) were identified (Fig. 7). The electrode precipitate retrieved at the end

**Table III. Summary of "Ash M" dissolved REE concentration at the end of EDR and comparison to REE found dissolved in distilled water and 0.01 mol $l^{-1}$ $Na_2SO_4$ solutions.**

| Solution REE | Distilled water (ug $l^{-1}$) | 0.01 mol $l^{-1}$ $Na_2SO_4$ (ug $l^{-1}$) | Coal#1 "Ash M" (ug $l^{-1}$) | Coal#2 "Ash M" (ug $l^{-1}$) | Coal#3 "Ash M" (ug $l^{-1}$) | ATL-5 "Ash M" (ug $l^{-1}$) |
|---|---|---|---|---|---|---|
| Y | 0.25 | <0.4 | 335.5 | 261.1 | 640.3 | 486.1 |
| Nd | 2.50 | <0.4 | 457.5 | 346.1 | 835.6 | 544.0 |
| Eu | 0.25 | <0.2 | 18.1 | 14.0 | 33.2 | 23.8 |
| Tb | 0.25 | <0.2 | 11.6 | 9.19 | 21.2 | 11.8 |
| Dy | 0.50 | <0.2 | 63.4 | 50.9 | 114.0 | 71.3 |
| Er | 0.25 | <0.2 | 31.3 | 24.7 | 55.7 | 38.2 |
| Ce | 5.00 | 0.41 | 860.6 | 636.9 | 1333.9 | 961.1 |
| Gd | 0.50 | <0.2 | 78.6 | 61.4 | 144.2 | 90.9 |
| La | 0.50 | <0.2 | 361.0 | 265.8 | 613.2 | 375.7 |
| Pr | 1.00 | <0.2 | 113.0 | 85.5 | 202.0 | 131.1 |
| Sm | 0.50 | <0.2 | 88.5 | 69.0 | 164.5 | 120.3 |
| Ho | 0.25 | <0.2 | 11.9 | 9.3 | 21.4 | 12.7 |
| Lu | 0.25 | <0.2 | 3.8 | 3.0 | 7.2 | 6.0 |
| Sc | 10.0 | <0.8 | 211.5 | 76.6 | 286.3 | 967.2 |
| Tm | 0.25 | <0.2 | 4.2 | 3.3 | 7.4 | 5.2 |
| Yb | 0.25 | <0.2 | 25.9 | 20.5 | 45.2 | 38.6 |

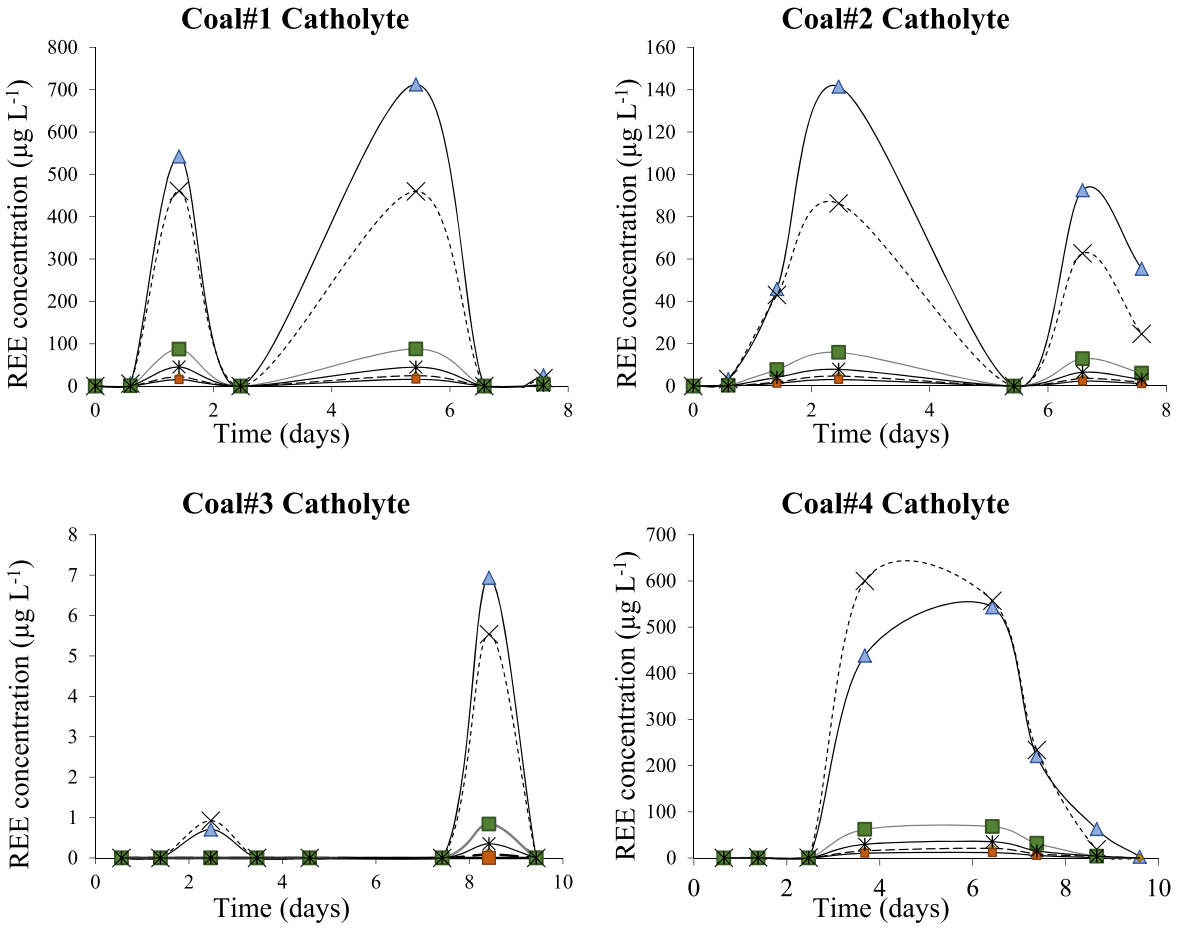


**Figure 5.** The breakthrough curves of the six critical REE (Nd, Y, Eu, Tb, Dy, and Er) at the outflow of the cathode reservoir. There is no initial lag time since the cathode reservoir is full at the start of the experiment.

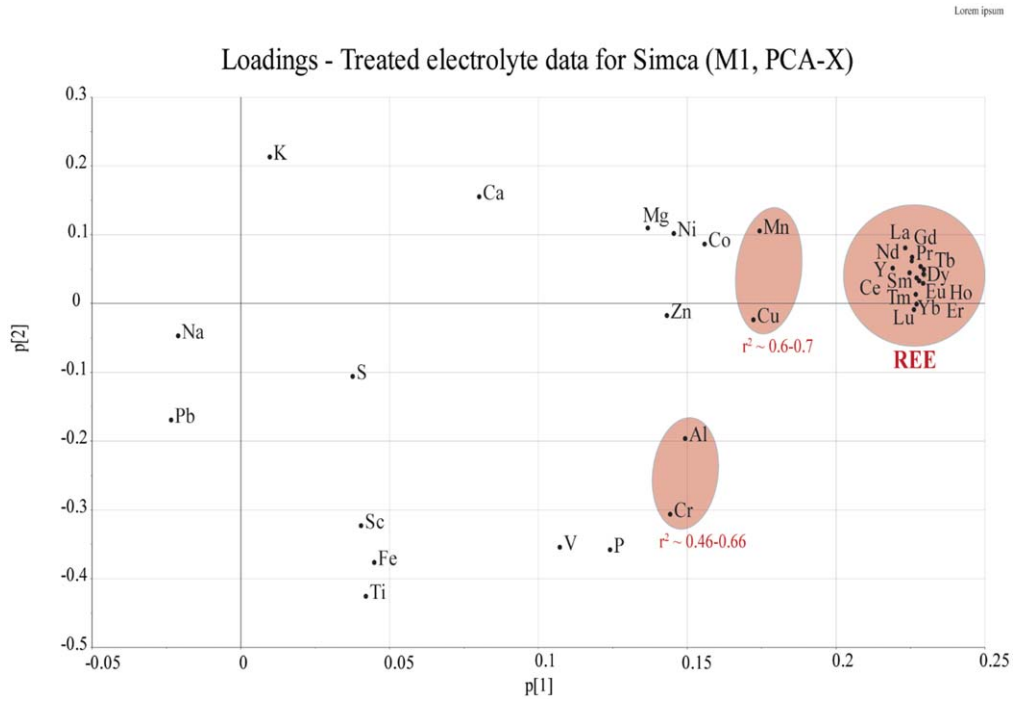


**Figure 6.** PCA plot of Coal#1-Coal#4 electrolyte Al, As, Ba, Cd, Cr, Cu, Fe, K, Mg, Mn, Na, Ni, P, Pb, S, Zn and REE (Sc, Y, La, Ce, Pr, Nd, Sm, Eu, Gd, Tb, Dy, Ho, Er, Tm, Yb, and Lu) concentrations. Red bubbles represent clusters of elements close between each other and closest to REEs. $r^2$ values are retrieved from the correlation matrix and define $r^2$ between REEs and the most significantly correlated elements: Mn, Cu, Al, and Cr.

**Table IV. REE diffusion coefficients retrieved from. Ref. 56.**

| REE list | $D_i$ ($cm^2\ s^{-1}$) | zi | $u_i^*$ ($cm^2\ V^{-1}\ s^{-1}$) | Coal#1 Ci (M final conc.) (mol $cm^{-3}$) | Coal#2 Ci (M final conc.) (mol $cm^{-3}$) | Coal#3 Ci (M final conc.) (mol $cm^{-3}$) | Coal#4 Ci (M final conc.) (mol $cm^{-3}$) | Coal#1 $J_i^m$ (mol $cm^{-2}\ s^{-1}$) | Coal#2 $J_i^m$ (mol $cm^{-2}\ s^{-1}$) | Coal#3 $J_i^m$ (mol $cm^{-2}\ s^{-1}$) | Coal#4 $J_i^m$ (mol $cm^{-2}\ s^{-1}$) |
|---|---|---|---|---|---|---|---|---|---|---|---|
| Y | N.A. | 3 | N.A. | $3.8{\cdot}10^{-3}$ | $2.9{\cdot}10^{-3}$ | $7.2{\cdot}10^{-3}$ | $5.5{\cdot}10^{-3}$ | | | | |
| Nd | $6.16{\cdot}10^{-6}$ | 3 | $7.29{\cdot}10^{-7}$ | $3.2{\cdot}10^{-3}$ | $2.4{\cdot}10^{-3}$ | $5.8{\cdot}10^{-3}$ | $3.8{\cdot}10^{-3}$ | $8.02{\cdot}10^{-10}$ | $1.12{\cdot}10^{-9}$ | $2.17{\cdot}10^{-9}$ | $1.26{\cdot}10^{-9}$ |
| Eu | $6.02{\cdot}10^{-6}$ | 3 | $7.12{\cdot}10^{-7}$ | $1.0{\cdot}10^{-4}$ | $8.35{\cdot}10^{-5}$ | $2.0{\cdot}10^{-4}$ | $1.0{\cdot}10^{-4}$ | $2.67{\cdot}10^{-11}$ | $3.81{\cdot}10^{-11}$ | $7.25{\cdot}10^{-11}$ | $4.65{\cdot}10^{-11}$ |
| Tb | $5.87{\cdot}10^{-6}$ | 3 | $6.94{\cdot}10^{-7}$ | $7.3{\cdot}10^{-5}$ | $5.78{\cdot}10^{-5}$ | $1.0{\cdot}10^{-4}$ | $7.42{\cdot}10^{-5}$ | $1.76{\cdot}10^{-11}$ | $2.57{\cdot}10^{-11}$ | $4.76{\cdot}10^{-11}$ | $2.37{\cdot}10^{-11}$ |
| Dy | $5.82{\cdot}10^{-6}$ | 3 | $6.89{\cdot}10^{-7}$ | $4.0{\cdot}10^{-4}$ | $3.1{\cdot}10^{-4}$ | $7.3{\cdot}10^{-4}$ | $4.0{\cdot}10^{-4}$ | $9.32{\cdot}10^{-11}$ | $1.38{\cdot}10^{-10}$ | $2.48{\cdot}10^{-10}$ | $1.39{\cdot}10^{-10}$ |
| Er | $5.85{\cdot}10^{-6}$ | 3 | $6.92{\cdot}10^{-7}$ | $2.1{\cdot}10^{-4}$ | $1.0{\cdot}10^{-4}$ | $3.0{\cdot}10^{-4}$ | $2.1{\cdot}10^{-4}$ | $4.49{\cdot}10^{-11}$ | $6.54{\cdot}10^{-11}$ | $1.18{\cdot}10^{-10}$ | $7.27{\cdot}10^{-11}$ |
| Ce | $6.19{\cdot}10^{-6}$ | 3 | $7.33{\cdot}10^{-7}$ | $6.1{\cdot}10^{-3}$ | $4.5{\cdot}10^{-3}$ | $9.5{\cdot}10^{-3}$ | $6.8{\cdot}10^{-3}$ | $1.56{\cdot}10^{-9}$ | $2.13{\cdot}10^{-9}$ | $3.58{\cdot}10^{-9}$ | $2.31{\cdot}10^{-9}$ |
| Gd | $5.97{\cdot}10^{-6}$ | 3 | $7.06{\cdot}10^{-7}$ | $5.0{\cdot}10^{-4}$ | $4.0{\cdot}10^{-4}$ | $9.0{\cdot}10^{-4}$ | $6.0{\cdot}10^{-4}$ | $1.22{\cdot}10^{-10}$ | $1.77{\cdot}10^{-10}$ | $3.33{\cdot}10^{-10}$ | $1.88{\cdot}10^{-10}$ |
| La | $6.19{\cdot}10^{-6}$ | 3 | $7.33{\cdot}10^{-7}$ | $2.6{\cdot}10^{-3}$ | $1.9{\cdot}10^{-3}$ | $4.4{\cdot}10^{-3}$ | $2.7{\cdot}10^{-3}$ | $6.60{\cdot}10^{-10}$ | $8.97{\cdot}10^{-10}$ | $1.66{\cdot}10^{-9}$ | $9.11{\cdot}10^{-10}$ |
| Pr | $6.18{\cdot}10^{-6}$ | 3 | $7.31{\cdot}10^{-7}$ | $8.0{\cdot}10^{-4}$ | $6.0{\cdot}10^{-4}$ | $1.4{\cdot}10^{-3}$ | $9.0{\cdot}10^{-4}$ | $2.03{\cdot}10^{-10}$ | $2.84{\cdot}10^{-10}$ | $5.38{\cdot}10^{-10}$ | $3.13{\cdot}10^{-10}$ |
| Sm | $6.08{\cdot}10^{-6}$ | 3 | $7.20{\cdot}10^{-7}$ | $6.0{\cdot}10^{-4}$ | $4.0{\cdot}10^{-4}$ | $1.2{\cdot}10^{-3}$ | $8.0{\cdot}10^{-4}$ | $1.47{\cdot}10^{-10}$ | $2.11{\cdot}10^{-10}$ | $4.04{\cdot}10^{-10}$ | $2.65{\cdot}10^{-10}$ |
| Ho | $5.88{\cdot}10^{-6}$ | 3 | $6.96{\cdot}10^{-7}$ | $7.22{\cdot}10^{-5}$ | $5.64{\cdot}10^{-5}$ | $1.0{\cdot}10^{-4}$ | $7.70{\cdot}10^{-5}$ | $1.74{\cdot}10^{-11}$ | $2.51{\cdot}10^{-11}$ | $4.64{\cdot}10^{-11}$ | $2.46{\cdot}10^{-11}$ |
| Lu | N.A. | 3 | N.A. | $2.17{\cdot}10^{-5}$ | $1.72{\cdot}10^{-5}$ | $4.12{\cdot}10^{-5}$ | $3.43{\cdot}10^{-5}$ | | | | |
| Sc | $5.74{\cdot}10^{-6}$ | 3 | $6.79{\cdot}10^{-7}$ | $4.7{\cdot}10^{-3}$ | $1.7{\cdot}10^{-3}$ | $6.4{\cdot}10^{-3}$ | $22.0{\cdot}10^{-3}$ | $1.11{\cdot}10^{-9}$ | $7.41{\cdot}10^{-10}$ | $2.22{\cdot}10^{-9}$ | $6.72{\cdot}10^{-9}$ |
| Tm | $5.8{\cdot}10^{-6}$ | 3 | $6.86{\cdot}10^{-7}$ | $2.49{\cdot}10^{-5}$ | $1.95{\cdot}10^{-5}$ | $4.38{\cdot}10^{-5}$ | $3.08{\cdot}10^{-5}$ | $5.92{\cdot}10^{-12}$ | $8.58{\cdot}10^{-12}$ | $1.54{\cdot}10^{-11}$ | $9.72{\cdot}10^{-12}$ |
| Yb | $5.82{\cdot}10^{-6}$ | 3 | $6.89{\cdot}10^{-7}$ | $1.0{\cdot}10^{-4}$ | $1.2{\cdot}10^{-4}$ | $2.6{\cdot}10^{-4}$ | $2.2{\cdot}10^{-4}$ | $3.57{\cdot}10^{-11}$ | $5.22{\cdot}10^{-11}$ | $9.24{\cdot}10^{-11}$ | $7.07{\cdot}10^{-11}$ |
| Electric field ($V\ cm^{-1}$) | | | | 0.35 | 0.64 | 0.51 | 0.46 | | | | |
| Current density ($A\ cm^{-2}$) | | | | 0.0012 | 0.0012 | 0.0012 | 0.0012 | | | | |

**Table V. Summary of electric field and current density resulting from the four EDR experiments. The cross section area stands for the EDR reactor area.**

| Experiment | Electric field (V) | Current (mA) | Cross section area ($m^2$) | Distance between electrodes (m) |
|---|---|---|---|---|
| Coal#1 | 5.2 ± 1.3 | 60 | 0.005 | 0.15 |
| Coal#2 | 9.6 ± 5.1 | 60 | 0.005 | 0.15 |
| Coal#3 | 7.7 ± 4.7 | 60 | 0.005 | 0.15 |
| Coal#4 | 6.9 ± 1.6 | 60 | 0.005 | 0.15 |

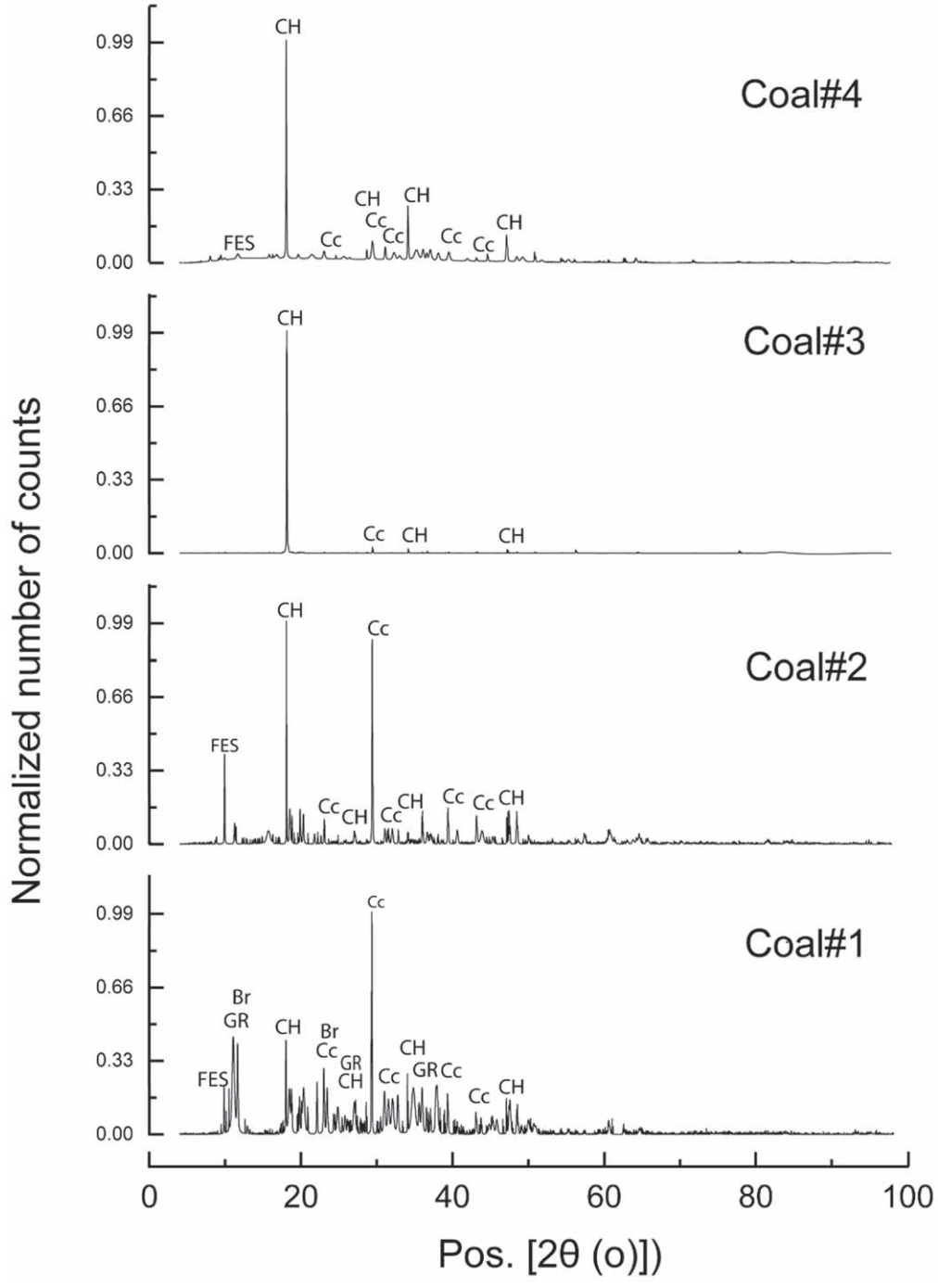


**Figure 7.** X-ray diffraction of powdered electrode precipitate after 48 h of drying after EDR experiments. Symbols stand for FES Iron Sulfate hydroxide, GR Green rust I, CH Calcium hydroxide, Cc Calcite, and Br Brushite.

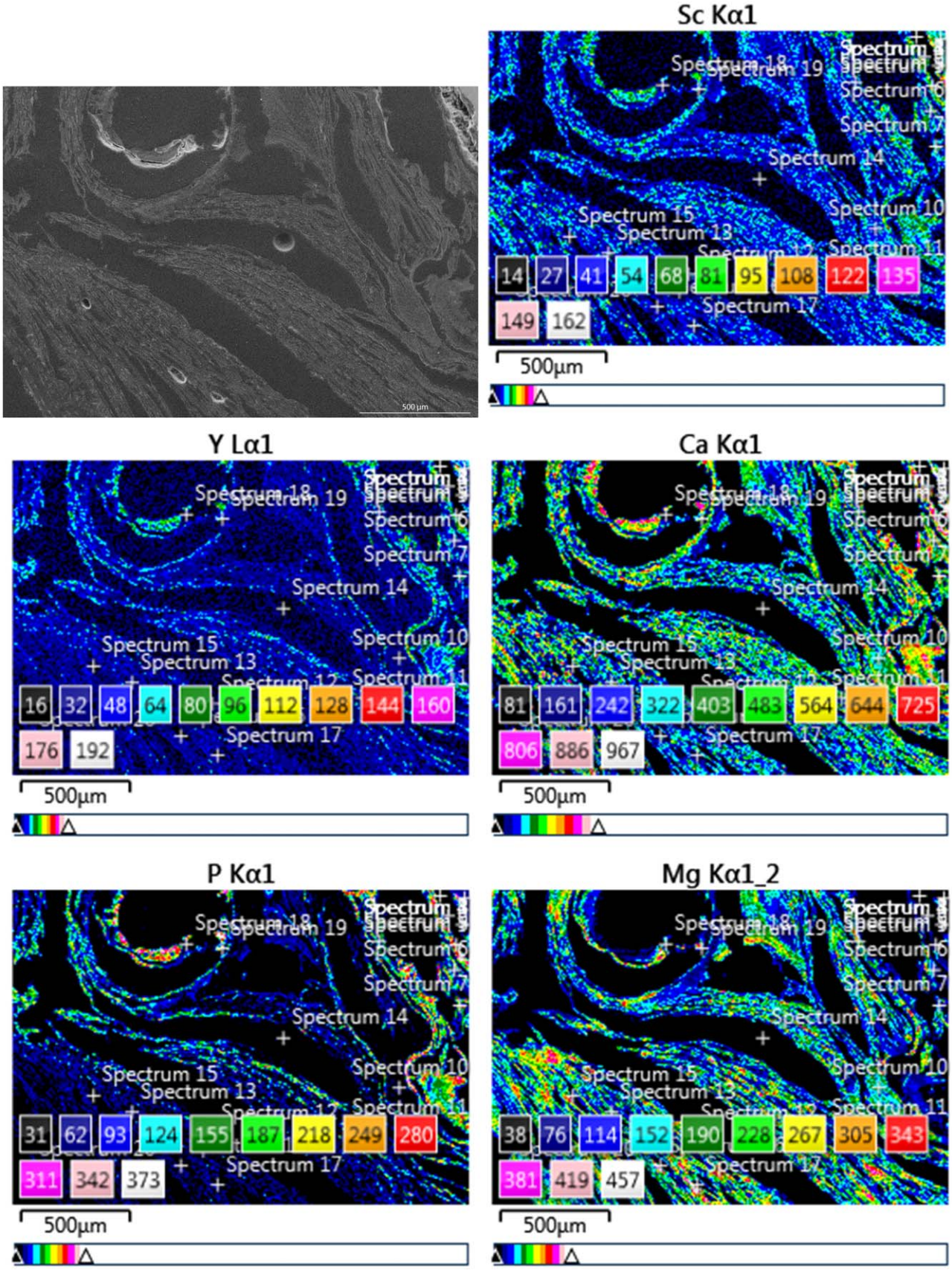


**Figure 8.** ESEM detail of electrode precipitation during experiment Coal#4. Use of ETD detector, at a 25.00 kV and pressure of 9.01e-5 Pa. (A) represents the overall cross-section layers at a lower resolution, where we can see the titanium electrode in the upper right corner of the figure.

**Table VI. REE represents the sum of the 16 REE analyzed in this study.**

| Experiment | Energy consumption (Wh) per 100 g of coal ash—Eq. 1[a)] | mg of REE extracted per 100 g of coal ash[b)] | Range of $J_i^m$ (mol $cm^{-2}$ $s^{-1}$): Lowest (REE); highest (REE)—Eq. 2 |
|---|---|---|---|
| Coal#1 | 57.45 | 5.38 | $5.92{\cdot}10^{-12}$ (Tm); $1.11{\cdot}10^{-9}$ (Sc) |
| Coal#2 | 96.77 | 1.48 | $8.58{\cdot}10^{-12}$ (Tm); $2.13{\cdot}10^{-9}$ (Ce) |
| Coal#3 | 77.62 | 3.04 | $1.54{\cdot}10^{-11}$ (Tm); $3.58{\cdot}10^{-9}$ (Ce) |
| Coal#4 | 69.55 | 14.78 | $9.72{\cdot}10^{-12}$ (Tm); $6.72{\cdot}10^{-9}$ (Sc) |

a) To this, we need to add 270 Wh per day of stirring device usage (Fig. 2). Retrieved from. Ref. 69. b) Sum of REE located at the catholyte, cation-exchange membrane, and cathode in the EDR cell at the end of the experiments.

of all Coal#1–4 did not show REE oxides in the mineralogy study, maybe because of the low REE contents compared to other competing cations. This means that the absence of REE oxides implies that no form of REE readily usable in producing e.g., strong magnets[9,60] was available. Indeed, aqueous REE electrodeposition at room temperature has been deemed unfeasible,[61] but recent studies have shown REE electrodeposition using ionic liquids.[62] In this study, we have observed REE electrodeposition (Figs. 4, 8). Coal#4 electrode was prepared in a cross-section for further investigations, as described in section 2.3. Elemental mapping of this cross-section allows us to understand the composition of the different layers and identify which layers encapsulate REEs. Because REE concentrations deposited at the electrode were reduced (Fig. 4, Table V), only Sc and Y had enough energy to present significant contrast in the ESEM (Fig. 8). We can observe that both Sc and Y have a high correlation with P and Ca (Fig. 8), suggesting that a P-bearing mineral adsorbs/encapsulates the REE at the time of electrodeposition—perhaps another calcium phosphate mineral since brushite was not detected in Coal#4 (Fig. 7). Literature shows that phosphogypsum, an industrial by-product of wet-process phosphoric acid production, is enriched with REE.[63,64] Phosphate deposits are an important REE ore[30] (see Fig. 1). REE is complexed into a P-bearing mineral and sinks REEs at the electrode may be counterproductive—since it has to be acid extracted once again for resource recovery. However, it readily solubilizes with a strong acid (5 mol $l^{-1}$ $HNO_3$, methods described in section 2.2).

***EDR efficiency for REE extraction from coal fly ashes.—*** Table VI summarizes EDR efficiency parameters. Regarding energy consumption, we are also on the lower end of the scale, where Sun et al.[41] estimated 180–270 Wh and 141 Wh in[65] per 100 g of treated materials. Any of the experiments Coal#1–4 consume less than 100 Wh per 100 g of treated coal ash, with the maximum energy efficiency of 57 Wh in Coal#1 (Table V). Coal#1 only delivers 20% REE extraction. Coal#4, on the other hand, extracts 40% of the REE and uses 70 Wh—still rather low in comparison to Ref. 65. Coal#4 extracts 148 g from 1 ton of coal ashes (calculated based on Table VI). As a lever, literature indicates that to obtain 1 tonne of REE from ore, 24.6 tonnes of raw ore are necessary.[66] This gives us an idea of the total REE recovery capacity achieved during EDR. Lastly, the ionic migration of REE $J_i^m$ is on the higher side (Table VI) as seen already in section 3.2. This paper comes at critical time, because coal fly ashes are phasing out production since coal combustion as an energy source has been banned by many countries.[67,68] Neverthelss the study still adds to the potential of using EDR as a REE extraction method.

## Conclusions

This study applied EDR to coal fly ash to extract REE in a circular, resource recovery approach. We suspended the ash in different solutions during EDR to understand the effect of REE speciation on EDR efficiency. Adding 0.01 mol $l^{-1}$ $NaNO_3$ (at pH2) (Coal#2) or 0.4 mol $l^{-1}$ Sodium acetate in 1.0 mol $l^{-1}$ Acetic acid (Coal#3) did not enhance REE mobility. Using merely distilled water (Coal#1), we achieved high removal efficiencies, but the best results were achieved with 0.5 mol $l^{-1}$ citric acid (Coal#4). This is because trivalent REEs form strong complexes with carboxylate,[59] making them mobile and hydrolyzed.[36,54] Coal#4 was the most promising experiment, achieving 40% REE extraction, mostly precipitated at the cathode. Indeed, once at the cathode compartment, REEs tend to precipitate at the electrode complexed with a Ca- and P-bearing mineral. Mineralogy analysis showed only brushite ($CaHPO_4{\cdot}2H_2O$) mineral as electrode precipitate in Coal#1, but ESEM mapping showed spatial overlapping between Sc, Y, Ca, and P elements. We then hypothesize that REE reprecipitates at the electrode as a P-bearing mineral. The conducted EDR experiments showed encouraging results, notwithstanding in need of optimization. Changing the solution, where the ash was suspended during the treatment, showed different REE extraction results. This gives basis for optimization. In the experiments, we found citric acid to be the most promising chemical, and optimization of the concentration should be conducted. In addition, the fact that the REEs precipitated at the cathode is also a good basis for optimization in relation to a separation process, where the precipitate contain a content of REEs for further processing (up to 30% of the 40% extracted REE in Coal#4).

## Acknowledgments

The research leading to these results has received funding from the European Union's Horizon 2020 research and innovation program under the Marie Sklodowska-Curie grant agreement no. 713683 (COFUNDfellowsDTU) for Ana T. Lima.

## ORCID

Ana T. Lima https://orcid.org/0000-0001-6980-6553

## References

1. X. Du and T. E. Graedel, *Sci. Total Environ.*, **461–462**, 781 (2013).
2. W. Zhang, M. Rezaee, A. Bhagavatula, Y. Li, J. Groppo, and R. Honaker, *Int. J. Coal Prep. Util.*, **35**, 295 (2015).
3. Y. Wu, X. Yin, Q. Zhang, W. Wang, and X. Mu, *Resour. Conserv. Recycl.*, **88**, 21 (2014).
4. S. Dai and R. B. Finkelman, *Int. J. Coal Geol.*, **186**, 155 (2018).
5. S. M. Jowitt, T. T. Werner, Z. Weng, and G. M. Mudd, *Curr. Opin. Green Sustain. Chem.*, **13**, 1 (2018).
6. G. Gaustad, E. Williams, and A. Leader, *Resour. Conserv. Recycl.*, **167**, 105213 (2021).
7. R. M. Izatt, S. R. Izatt, R. L. Bruening, N. E. Izatt, and B. A. Moyer, *Chem. Soc. Rev.*, **43**, 2451 (2014).
8. B. K. Reck and T. E. Graedel, *Science (80-.).*, **337**, 690 (2012).
9. K. Binnemans, P. T. Jones, B. Blanpain, T. Van Gerven, Y. Yang, A. Walton, and M. Buchert, *J. Clean. Prod.*, **51**, 1 (2013).
10. D. H. Dang, K. A. Thompson, L. Ma, H. Q. Nguyen, S. T. Luu, M. T.-N. Duong, and A. Kernaghan, *Arch. Environ. Contam. Toxicol.*, **81**, 521 (2021).
11. A. T. Lima and L. Ottosen, *Chemosphere*, **265**, 129163 (2020).
12. John Rankin, *Minerals, Metals and Sustainability: Meeting Future Material Needs* (CSIRO Publishing , Clayton, CA) (2011), http://hdl.handle.net/102.100.100/103261?index=1.
13. P. Anastas and N. Eghbali, *Chem. Soc. Rev.*, **39**, 301 (2010).
14. N. Couto, A. R. Ferreira, V. Lopes, S. C. Peters, E. P. Mateus, A. B. Ribeiro, and S. Pamukcu, *Electrochim. Acta*, **359**, 136934 (2020).
15. S. Maes, W. Q. Zhuang, K. Rabaey, L. Alvarez-Cohen, and T. Hennebel, *Environ. Sci. Technol.*, **51**, 1654 (2017).
16. A. T. Lima, P. C. Rodrigues, and J. T. Mexia, *J. Hazard. Mater.*, **175**, 366 (2010).
17. P. Guedes, N. Couto, L. M. Ottosen, G. M. Kirkelund, E. Mateus, and A. B. Ribeiro, *Waste Manag.*, **52**, 193 (2016).
18. V. V. Seredin and S. Dai, *Int. J. Coal Geol.*, **94**, 67 (2012).
19. J. Pan, B. V. Hassas, M. Rezaee, C. Zhou, and S. V. Pisupati, *J. Clean. Prod.*, **284**, 124725 (2021).
20. A. Middleton, D. M. Park, Y. Jiao, and H. Hsu-Kim, *Int. J. Coal Geol.*, **227**, 103532 (2020).
21. M. L. D. Jayaranjan, E. D. van Hullebusch, and A. P. Annachhatre, *Rev. Environ. Sci. Bio/Technology*, **13**, 467 (2014).
22. M. U. Hossain, C. S. Poon, I. M. C. Lo, and J. C. P. Cheng, *Resour. Conserv. Recycl.*, **120**, 199 (2017).
23. D. Sengupta and S. Agrahari, *Modelling Trends in Solid and Hazardous Waste Management* (Springer, Singapore) p. 15 (2017).
24. S. Kashiwakura, Y. Kumagai, H. Kubo, and K. Wagatsuma, *Open J. Phys. Chem.*, **2013**, 69 (2013).
25. Prakash Joshi B. et al., *United States Patent*, Recovery of rare earth elements and compounds from coal ash (2013), https://patents.google.com/patent/US8968688/en.
26. S. Costis, K. K. Mueller, L. Coudert, C. M. Neculita, N. Reynier, and J. F. Blais, *J. Geochemical Explor.*, **221**, 106699 (2021).
27. V. Innocenzi, F. Ferella, I. de Michelis, and F. Vegliò, *J. Ind. Eng. Chem.*, **24**, 92 (2015).
28. M. Case, R. Fox, D. Baek, and C. Wai, *Met.*, **9**, 429 (2019).
29. C. R. Borra, Y. Pontikes, K. Binnemans, and T. Van Gerven, *Miner. Eng.*, **76**, 20 (2015).
30. I. De Michelis, F. Ferella, E. F. Varelli, and F. Vegliò, *Waste Manag.*, **31**, 2559 (2011).
31. B. M. Cieślik, J. Namieśnik, and P. Konieczka, *J. Clean. Prod.*, **90**, 1 (2015).
32. B. Ebbers, L. M. Ottosen, and P. E. Jensen, *Chemosphere*, **125**, 122 (2015).
33. T. Scarazzato, Z. Panossian, J. A. S. Tenório, V. Pérez-Herranz, and D. C. R. Espinosa, *J. Clean. Prod.*, **168**, 1590 (2017).
34. L. M. Ottosen, P. E. Jensen, and G. M. Kirkelund, *Sep. Sci. Technol.*, **49**, 1910 (2014).

35. L. M. Ottosen, A. T. Lima, A. J. Pedersen, and A. B. Ribeiro, *J. Chem. Technol. Biotechnol.*, **81**, 553 (2006).
36. C. M. G. Pires, H. D. A. Ponte, J. T. Pereira, and M. J. J. D. S. Ponte, *J. Clean. Prod.*, **227**, 272 (2019).
37. J. H. L. Voncken, *The Rare Earth Elements An Introduction* (Springer: Briefs in Earth Science, Delft) p. 137 (2016).
38. G. M. Kirkelund, P. E. Jensen, L. M. Ottosen, and K. B. Pedersen, *J. Hazard. Mater.*, **367**, 68 (2019).
39. H. Nguyen, W. Kunther, K. Gijbels, P. Samyn, V. Carvelli, M. Illikainen, and P. Kinnunen, *Cem. Concr. Res.*, **140**, 106315 (2021).
40. I. T. Jolliffe, *Principal Component Analysis* (Springer, New York, NY) p. 1 (2002).
41. T. R. Sun, L. M. Ottosen, P. E. Jensen, and G. M. Kirkelund, *Electrochim. Acta*, **107**, 187 (2013).
42. M. P. Ketris and Y. E. Yudovich, *Int. J. Coal Geol.*, **78**, 135 (2009).
43. N. M. Sigvardsen and L. M. Ottosen, *Cem. Concr. Compos.*, **95**, 25 (2019).
44. M. B. Folgueras, R. M. Díaz, J. Xiberta, and I. Prieto, *Fuel*, **82**, 1939 (2003).
45. M. B. Folgueras, M. Alonso, and F. J. Fernández, *Fuel*, **192**, 128 (2017).
46. K. W. Goyne, S. L. Brantley, and J. Chorover, *Chem. Geol.*, **278**, 1 (2010).
47. R. Ding and S. A. Wood, "The aqueous geochemistry ofthe rare earth elements and yttrium. Part X. Potentiometric determination of stability constants ofacetate complexes of La3+, Nd3+, Gd3+ and Yb3+ at 25-70 °C and 1 bar." *Water-Rock Interactions, Ore Deposits, and Environmental Geochemistry: A Tribute to David A Crerar*, ed. Roland Hellmann and Scott A Wood (The Geochemical Society, Special Publication No.7,, Washington DC) (2002), No.7.
48. T. Hirato, *Treatise on Process Metallurgy*, **1**, 653 (2013).
49. A. N. Alshawabkeh and Y. B. Acar, *J. Environ. Sci. Heal.. Part A Environ. Sci. Eng. Toxicol.*, **27**, 1835 (1992).
50. K. B. Pedersen, L. M. Ottosen, P. E. Jensen, and T. Lejon, *Electrochim. Acta*, **181**, 48 (2015).
51. T. Rabung, T. Stumpf, H. Geckeis, R. Klenze, and J. I. Kim, *Radiochim. Acta*, **88**, 711 (2000).
52. U. M. Sutopo, E. R. Desfitri, Y. Hayakawa, and S. Kambara, *Minerals*, **11**, 1270 (2021).
53. S. Park, M. Kim, Y. Lim, J. Yu, S. Chen, S. W. Woo, S. Yoon, S. Bae, and H. S. Kim, *J. Hazard. Mater.*, **402**, 123760 (2021).
54. S. I. Arbuzov, S. G. Maslov, R. B. Finkelman, A. M. Mezhibor, S. S. Ilenok, M. G. Blokhin, and E. V. Peregudina, *J. Geochemical Explor.*, **184**, 40 (2018).
55. Y. B. Acar, R. J. Gale, A. N. Alshawabkeh, R. E. Marks, S. Puppala, M. Bricka, and R. Parker, *J. Hazard. Mater.*, **40**, 117 (1995).
56. M. S. Liyananadirah, M. R. Deraman, W. H. Ibrahim, and N. Harun, *IOP Conf. Ser.: Mater. Sci. Eng.*, **702**, 012045 (2019).
57. J. K. Mitchell, *Fundamentals of Soil Behavior* (Wiley, New York, NY) (1993).
58. A. T. Lima, L. M. Ottosen, K. Heister, and J. P. G. Loch, *Sci. Total Environ.*, **435–436**, 1 (2012).
59. S. A. Wood, *Eng. Geol.*, **34**, 229 (1993).
60. W. Chen, J. Jiang, X. Lan, X. Zhao, H. Mou, and T. Mu, *Green Chem.*, **21**, 4748 (2019).
61. T. E. Lister, P. Wang, and A. Anderko, *Hydrometallurgy*, **149**, 228 (2014).
62. E. Bourbos, I. Giannopoulou, A. Karantonis, D. Panias, and I. Paspaliaris, *ERES2014: 1st European Rare Earth Resources Conference*, p. 7 (2014).
63. H. Liang, P. Zhang, Z. Jin, and D. DePaoli, *Miner. Metall. Process*, **34**, 201 (2017).
64. J. L. Mukaba, C. P. Eze, O. Pereao, and L. F. Petrik, *Minerals*, **11**, 1051 (2021).
65. X. Zhan and G. M. Kirkelund, *J. Hazard. Mater.*, **412**, 125220 (2021).
66. L. Talens Peiró and G. V. Méndez, *JOM*, **65**, 1327 (2013).
67. IPCC, *Climate Change 2021: The Physical Science Basis. Contribution of Working Group I to the Sixth Assessment Report of the Intergovernmental Panel on Climate Change*, Intergovernmental Panel on Climate Change (2021) p. 3949, Cambridge University Press Working Group IPCCR, https://www.ipcc.ch/report/ar6/wg1/#SPM.
68. UNCC, End of Coal in Sight at COP, 26 (https://unfccc.int/news/end-of-coal-in-sight-at-cop26).
69. V. Oliveira, G. M. Kirkelund, C. Horta, J. Labrincha, and C. Dias-Ferreira, *Appl. Energy*, **247**, 182 (2019).